Published in final edited form as:
J Am Chem Soc. 2010 August 11; 132(31): 10638–10641. doi:10.1021/ja104859j.

Tailoring DNA Structure To Increase Target Hybridization Kinetics on Surfaces

Andrew E. Prigodich, **One-Sun Lee**, **Weston L. Daniel**, **Dwight S. Seferos**, **George C. Schatz**, and **Chad A. Mirkin***
Department of Chemistry and International Institute for Nanotechnology, Northwestern University, 2145 Sheridan Road, Evanston, Illinois 60208-3113

Abstract

We report a method for increasing the rate of target hybridization on DNA-functionalized surfaces using a short internal complement DNA (sicDNA) strand. The sicDNA causes up to a 5-fold increase in association rate by inducing a conformational change that extends the DNA away from the surface, making it more available to bind target nucleic acids. The sicDNA-induced kinetic enhancement is a general phenomenon that occurred with all sequences and surfaces investigated. Additionally, the process is selective and can be used in multicomponent systems to controllably and orthogonally "turn on" specific sequences by the addition of the appropriate sicDNA. Finally, we show that sicDNA is compatible with systems used in gene regulation, intracellular detection, and microarrays, suggesting several potential therapeutic, diagnostic, and bioinformatic applications.

There is a major need to increase the rate of DNA hybridization on surfaces in order to improve the speed and efficiency of bioinformatic assays, diagnostics, and therapeutic agents.[1] Such methods should not only be easily employable and compatible with a wide range of sequences but also retain their activity both inside and outside a cellular environment. Previous approaches for increasing DNA hybridization rates include the use of designer nucleic acids[2] and hairpin disruption.[3] However, designer nucleic acids are costly to synthesize, and hairpin disruption is incompatible with many sequences and applications. An alternative approach for increasing binding rates is the use of a region of double-stranded DNA (dsDNA) adjacent to a single-stranded DNA (ssDNA) target hybridization site.[4] The dsDNA region creates an additional base-stacking interaction with the incoming target, thereby stabilizing hybridization. It has also been proposed that structural changes caused by the dsDNA region could increase target hybridization kinetics on the surface of a nanoparticle.[5] However, previous work in this area has been performed on materials that allow both structural changes and base-stacking interactions to occur, making it difficult to experimentally distinguish the two factors.[4a,d,5] In addition to questions about the mechanism of action, the adjacent duplex strategy has several limitations. It has not been used to selectively "turn on" the hybridization of a specific sequence in a solution of many targets and capture sequences, and it is poorly suited for *in situ* biological applications. Thus, there remains a need for a general approach to dynamically control the rate of DNA hybridization both inside and outside of cells.

*chadnano@northwestern.edu.

Supporting Information Available: Methods and additional data. This material is available free of charge via the Internet at http://pubs.acs.org.

One class of materials where DNA hybridization is particularly important is a DNA-functionalized gold nanoparticle (DNA–Au NP), which consists of a spherical gold core with a dense monolayer of DNA covalently bound to the gold surface.[6] The unique architecture of DNA–Au NPs results in cooperative hybridization,[7] resistance to nucleases,[8] and extraordinary cellular uptake.[9] This combination of hybridization and cellular properties has proven useful in materials self-assembly,[6,10] extracellular diagnostics,[11] intracellular biodetection,[12] and gene regulation.[13] The intracellular utility of DNA–Au NPs provides an ideal platform for applying new types of hybridization control in biologically relevant systems. Our group has recently developed Nano-Flares, a class of DNA–Au NP that can detect mRNA levels inside a living cell[14] with high sensitivity relative to molecular beacons.[15] In this system, DNA–Au NPs are hybridized with a fluorophore-labeled short internal complement DNA (sicDNA). When sicDNA is bound, the gold surface quenches the fluorophore; upon target binding, the sicDNA is displaced, resulting in an increase in the fluorescence signal. This approach allows extremely sensitive *in situ* detection of unlabeled target mRNA. A major concern in the original Nano-Flare design was that the sicDNA would act as a competitive inhibitor and slow target binding. However, in the work presented here, we were able to quantitatively determine that sicDNA is not in fact a competitive inhibitor but rather acts cooperatively with the surface-bound DNA to increase the rate of target association. This result explains in part the remarkable efficiency of the Nano-Flare.[14] Furthermore, we have investigated the mechanism of rate enhancement and compared it to previously described systems. The proposed mechanism involves a structural change in the DNA that moves the ssDNA binding domain away from the surface, making it more available to the incoming target (Figure 1a). Unlike previous studies,[5] we were able to separate the roles of structural changes and base stacking because sicDNA is released during the target binding process, making base-stacking interactions unable to stabilize the final duplex. Additionally, the structural change is unique to sicDNA-bound strands, allowing us to orthogonally “turn on” the binding kinetics for specific sequences in multicomponent systems. This process not only plays an important role in Nano-Flare-based detection of mRNA and gene regulation[14,16] but also can be applied to microarray experiments, demonstrating the generality of the approach. This work suggests that our method for increasing DNA hybridization rates will be important in a wide range of fields, including bioinformatics, diagnostics, and therapeutics.

Au NPs (13 ± 1 nm) were synthesized by citrate reduction of $HAuCl_4$ and subsequently functionalized with DNA containing a 3′ propylthiol-A_{10} spacer and a 5′ 20-base-pair recognition region.[17] After purification from excess oligonucleotides, there were on average 73 ± 18 DNA strands per NP, as determined using a commercial DNA concentration assay.[18] Complementary DNA was then hybridized to the DNA–Au NPs. The efficient distance-dependent quenching of the gold surface was used to monitor the hybridization rate of DNA–Au NPs with fluorophore-labeled targets.

The rate of target hybridization to the DNA–Au NPs was measured with ssDNA–Au NPs or with DNA–Au NPs in the presence of one of four unlabeled complements [sicDNA, short external complement DNA (secDNA), long internal complement DNA (licDNA), and full complement DNA (fcDNA)] (Figure 1a). In these experiments, the labeled target and the unlabeled complement can both bind to the same region of DNA. In contrast to previous kinetic experiments[4,5] (see above), this prohibits the simultaneous binding of sicDNA and target to the same capture strand, preventing any additional base-stacking interactions from occurring. As expected, long unlabeled complements (licDNA and fcDNA) act as competitive inhibitors, greatly reducing the observed rate of association (k_{obs} = 0.0020 ± 0.0001 and 0.0008 ± 0.0002 min^{-1}, respectively) in comparison with ssDNA–Au NPs (0.011 ± 0.002 min^{-1}) (Figure 1b). Since sicDNA also binds in the target hybridization site, one might expect it to act as a competitive inhibitor as well; however, this DNA architecture

actually increases the rate of target binding (k_{obs} = 0.030 ± 0.002 min^{-1}) in comparison with ssDNA–Au NPs. Similar experiments were repeated with other DNA sequences and locked nucleic acid (LNA)–DNA chimeras. In all cases, a significant rate enhancement was observed when sicDNA was used (Figure 1 and Figure S1 in the Supporting Information), indicating that this is a general strategy for increasing the hybridization rate that is applicable to a wide range of DNA designs. Additionally, the effect of complement position was investigated by measuring the rate of target hybridization in the presence of short external duplexes with the same predicted binding strength as the sicDNA. Unlike the internal complements, the external complements had no significant effect on the hybridization rate (k_{obs} = 0.010 ± 0.002 min^{-1}) (Figure 1b), indicating that leaving an external ssDNA binding site available for incoming target is critical for the rate enhancement observed with sicDNA. Together, these results show that although most unlabeled complements inhibit the hybridization of a labeled target, the use of sicDNA results in more rapid binding. In particular, the combination of an internal dsDNA region with a relatively long ssDNA region (~9 base pairs) appears to be important for the rate increase.

We next investigated k_{obs} as a function of the number of sicDNA strands per Au NP. In all of these experiments, the number of available binding sites on the DNA–Au NPs exceeded the number of target molecules in solution. Under these conditions, the reaction reaches equilibrium with approximately 100% of the target bound.[7] The rate of association increases as a function of sicDNA concentration (Figure 1c). The hybridization rate plateaus as the concentration of sicDNA approaches the concentration of DNA covalently bound to the Au NP, reaching a maximum k_{obs} that is 4.7-fold larger than that for an ssDNA–Au NP, consistent with a rate-enhancing DNA structural change at the nanoparticle surface.

In order to further characterize the kinetics of the system, the relative contribution of k_{on} and k_{off} to the change in k_{obs} was investigated. These parameters were calculated for nanoparticles at three different concentrations of sicDNA (0, 20, and 50 sicDNA/NP) (Figure S2). Conjugates with 50 sicDNA strands per NP were found to have 5-fold larger k_{on} than ssDNA–Au NPs (k_{on} = 0.009 ± 0.004, 0.033 ± 0.004, and 0.045 ± 0.003 nM^{-1} min^{-1}, respectively, for the three concentrations). No significant difference in k_{off} was observed for any of the DNA–Au NPs under these conditions.

We next investigated whether the increased association rate was due to the DNA structure alone or a cooperative event involving the combined architecture of the DNA strands immobilized on a surface. The rate of DNA hybridization in the absence of Au NPs was measured using a molecular quencher in place of the gold nanoparticle, and the value of k_{obs} was found to be 58% smaller than that for the ssDNA–Au NPs. Kinetic measurements showed that the addition of sicDNA caused no observable change in rate when the DNA was not bound to the particle surface (Figure 1d), which is consistent with previous studies using similar DNA structures.[19] From this we conclude that the sicDNA-induced rate enhancement is a cooperative property arising from the combined architecture of the sicDNA and the nanoparticle surface. This distinguishes sicDNA from the previous techniques for increasing hybridization kinetics, as neither hairpin disruption[3] nor base-stacking[4a,d,5] mechanisms are surface-specific.

The sicDNA–Au NP conjugates contain two distinct types of binding sites: sicDNA-bound sites and unbound ssDNA sites. The origin of this rate increase could involve alteration of the DNA conformation specifically on the sicDNA-bound strand, thereby increasing the hybridization rate at that site. Alternately, sicDNA could change the conformation of DNA globally across the nanoparticle surface, thereby increasing the rate at both sicDNA-bound and unbound ssDNA sites. To distinguish these possibilities, Au NPs were functionalized

with two different DNA sequences, each having its own sicDNA and target, creating a mixed monolayer of DNA on the nanoparticle surface (Figure 2a). If sicDNA increases the binding rate to all nanoparticle-bound DNA, one would expect the addition of a single sicDNA sequence to increase the hybridization rate for both targets on the same nanoparticle. However, the results of these experiments show that sicDNA specifically increases the hybridization rate for its corresponding target and has no effect on the other target sequence (Figure 2b,c). In order to increase the hybridization rate of both targets simultaneously, both sicDNAs were required. This observation suggests that targets bind sicDNA sites preferentially over ssDNA sites on the nanoparticle surface. This was confirmed by monitoring the release of sicDNA as a function of added target (Figure S3). These results demonstrate that we can selectively "turn on" the target binding kinetics for a specific sequence even in a mixed monolayer of DNA, opening the door for applications in complex, multicomponent systems.

To determine whether sicDNA has an effect on the overall structure of the DNA–Au NPs, dynamic light scattering (DLS) was used to measure the hydrodynamic radii of the nanoparticles (Figure 3a). At high loadings of sicDNA, the radius increased by as much as 2.5 ± 0.9 nm, consistent with a sicDNA-induced structural change. Although the DLS experiment provides information about the general DNA–Au NP structure, specific regions of the DNA appear to be particularly important in increasing the hybridization rate. A relatively long region of ssDNA must be present on the external end of the DNA–Au NP (Figure 1b). To directly investigate the position of this external DNA region, the DNA covalently bound to the nanoparticle surface was labeled on the distal end with a fluorophore, and the nanoparticle-associated fluorescence was measured before and after the addition of sicDNA strands. When sicDNA was added to the DNA–Au NPs, an increase in fluorescence was observed, which can be attributed to an increase in the distance between the distal DNA end and the nanoparticle surface[20] (Figure 3b). This result, combined with the observed change in nanoparticle radius (Figure 3a) and the requirement of a distal ssDNA region in the sicDNA architecture (Figure 1), suggests that sicDNA acts by extending the ssDNA region away from the Au NP surface, making it more available to incoming targets.

The sicDNA-induced change in surface architecture was further investigated through molecular dynamics (MD) simulations. A flat gold surface was modeled with either seven ssDNA (Figure 4a) or seven sicDNA (Figure 4b) strands bound (see the Supporting Information for methods). When the sicDNA is present, the distance between the terminal base and the gold surface is increased by 1.2 ± 1.3 nm (Figure 4c), within one standard deviation of the increase measured by DLS. The modeling results, combined with the experimental structural studies (Figure 3), establish that sicDNA causes a conformational change in which the height of the DNA monolayer is increased, moving the terminal ssDNA region away from the particle surface. This agrees with previous simulations of DNA on gold surfaces[21] and suggests that the movement of the terminal ssDNA region increases its availability for target binding, thereby causing the observed increase in target binding rate.

The increase in hybridization rate observed with sicDNA–Au NPs may be general across a wide range of surface-based DNA technologies. The role of DNA density was investigated, as many of the unique cooperative binding properties of the DNA–Au NPs[7,9] arise because the DNA monolayer is much more dense than those on traditional flat surfaces. To test whether density plays a role in the hybridization kinetics, DNA–Au NPs were created with 85% fewer DNA strands per nanoparticle relative to the DNA–Au NPs described above.[9] The k_{obs} for target binding on the sparsely functionalized nanoparticles was much higher in the presence of sicDNA, indicating that high DNA density is not critical for the sicDNA-based rate increase (Figure S4). To further investigate the generality of sicDNA-induced

binding rate increases, we performed analogous binding rate experiments on microarrays. A microarray was created with ssDNA and sicDNA spots in different locations (Figure 5a). Fluorophore-labeled target DNA was hybridized to the chip, after which the fluorescence associated with each spot was quantified as a function of time and the initial hybridization rate determined (Figure 5b). We observed a 2-fold increase in initial binding rate with sicDNA. Although the increase is not as great as that observed on the DNA–Au NPs, this result still confirms that sicDNA can be used to increase the rate of hybridization on both high- and low-DNA-density surfaces and thus should be compatible with a wide range of applications, including intracellular detection, gene regulation, and microarrays.

Due to its nanoscale structure and its dynamic and controllable target binding properties, DNA plays an increasingly important role in a wide range of fields and in the development of new technologies. Control of DNA hybridization kinetics in the context of functional devices and materials will be needed for continued improvement and growth in this area. sicDNA induces changes in DNA surface structure that result in the presentation of an external ssDNA site that can easily initiate target binding, thereby increasing the overall rate of target hybridization. By addition of specific sicDNA sequences, the binding of a target can be selectively “turned on”, even in the presence of multiple sequences and targets. sicDNA increases the rate of target hybridization for all of the nucleic acids and surfaces tested, including microarrays and DNA–Au NPs, which can be used for intracellular experiments such as mRNA detection[14] and gene regulation.[13a] This work represents a significant step forward in the understanding of hybridization kinetics on surfaces and opens new doors for the development of advanced materials, biological assays, and medical devices.

Supplementary Material

Refer to Web version on PubMed Central for supplementary material.

Acknowledgments

This research was supported by the National Science Foundation (Grant CHE-0843832), the Northwestern NSEC Center NSF (Grant EEC-0647560), and the Northwestern Center for Cancer Nanobiotechnology Excellence (1 U54 CA119341-01). In addition, C.A.M. is grateful for an NSSEF Fellowship from the DoD, and A.E.P. was supported by a Ryan Fellowship.

References

(1) (a). Wang K, Tang Z, Yang CJ, Kim Y, Fang X, Li W, Wu Y, Medley CD, Cao Z, Li J, Colon P, Lin H, Tan W. Angew. Chem., Int. Ed. 2009; 48:856–870.(b) Moses S, Brewer SH, Lowe LB, Lappi SE, Gilvey LBG, Sauthier M, Tenent RC, Feldheim DL, Franzen S. Langmuir. 2004; 20:11134–11140. [PubMed: 15568868] (c) Katz E, Willner I. Angew. Chem., Int. Ed. 2004; 43:6042–6108.(d) Rosi NL, Mirkin CA. Chem. Rev. 2005; 105:1547–1562. [PubMed: 15826019] (e) Bath J, Turberfield AJ. Nat. Nanotechnol. 2007; 2:275–284. [PubMed: 18654284]

(2) (a). Wang L, Yang CYJ, Medley CD, Benner SA, Tan WH. J. Am. Chem. Soc. 2005; 127:15664–15665. [PubMed: 16277483] (b) Castoldi M, Schmidt S, Benes V, Noerholm M, Kulozik AE, Hentze MW, Muckenthaler MU. RNA. 2006; 12:913–920. [PubMed: 16540696]

(3) (a). Seelig G, Yurke B, Winfree E. J. Am. Chem. Soc. 2006; 128:12211–12220. [PubMed: 16967972] (b) Wei HR, Kuan PF, Tian SL, Yang CH, Nie J, Sengupta S, Ruotti V, Jonsdottir GA, Keles S, Thomson JA, Stewart R. Nucleic Acids Res. 2008; 36:2926–2938. [PubMed: 18385155] (c) Gao Y, Wolf LK, Georgiadis RM. Nucleic Acids Res. 2006; 34:3370–3377. [PubMed: 16822858] (d) Wang YF, Zhang Y, Ong NP. Phys. Rev. E. 2005; 72:051918.(e) Leunissen ME, Dreyfus R, Cheong FC, Grier DG, Sha R, Seeman NC, Chaikin PM. Nat. Mater. 2009; 8:590–595. [PubMed: 19525950]

(4) (a). Riccelli PV, Merante F, Leung KT, Bortolin S, Zastawny RL, Janeczko R, Benight AS. Nucleic Acids Res. 2001; 29:996–1004. [PubMed: 11160933] (b) Yuan BF, Zhuang XY, Hao YH, Tan Z. Chem. Commun. 2008:6600–6602.(c) Vasiliskov VA, Prokopenko DV, Mirzabekov AD. Nucleic Acids Res. 2001; 29:2303–2313. [PubMed: 11376149] (d) O'Meara D, Nilsson P, Nygren PA, Uhlen M, Lundeberg J. Anal. Biochem. 1998; 255:195–203. [PubMed: 9451504]

(5). Maye MM, Nykypanchuk D, van der Lelie D, Gang O. J. Am. Chem. Soc. 2006; 128:14020–14021. [PubMed: 17061872]

(6). Mirkin CA, Letsinger RL, Mucic RC, Storhoff JJ. Nature. 1996; 382:607–609. [PubMed: 8757129]

(7). Lytton-Jean AKR, Mirkin CA. J. Am. Chem. Soc. 2005; 127:12754–12755. [PubMed: 16159241]

(8). Seferos DS, Prigodich AE, Giljohann DA, Patel PC, Mirkin CA. Nano Lett. 2009; 9:308–311. [PubMed: 19099465]

(9). Giljohann DA, Seferos DS, Patel PC, Millstone JE, Rosi NL, Mirkin CA. Nano Lett. 2007; 7:3818–3821. [PubMed: 17997588]

(10) (a). Alivisatos AP, Johnsson KP, Peng XG, Wilson TE, Loweth CJ, Bruchez MP, Schultz PG. Nature. 1996; 382:609–611. [PubMed: 8757130] (b) Park SY, Lytton-Jean AKR, Lee B, Weigand S, Schatz GC, Mirkin CA. Nature. 2008; 451:553–556. [PubMed: 18235497]

(11)(a). Elghanian R, Storhoff JJ, Mucic RC, Letsinger RL, Mirkin CA. Science. 1997; 277:1078–1081. [PubMed: 9262471] (b) Park SJ, Taton TA, Mirkin CA. Science. 2002; 295:1503–1506. [PubMed: 11859188]

(12) (a). Zheng D, Seferos DS, Giljohann DA, Patel PC, Mirkin CA. Nano Lett. 2009; 9:3258–3261. [PubMed: 19645478] (b) Prigodich AE, Seferos DS, Massich MD, Giljohann DA, Lane BC, Mirkin CA. ACS Nano. 2009; 3:2147–2152. [PubMed: 19702321]

(13) (a). Rosi NL, Giljohann DA, Thaxton CS, Lytton-Jean AKR, Han MS, Mirkin CA. Science. 2006; 312:1027–1030. [PubMed: 16709779] (b) Patel PC, Giljohann DA, Seferos DS, Mirkin CA. Proc. Natl. Acad. Sci. U.S.A. 2008; 105:17222–17226. [PubMed: 19004812] (c) Giljohann DA, Seferos DS, Prigodich AE, Patel PC, Mirkin CA. J. Am. Chem. Soc. 2009; 131:2072–2073. [PubMed: 19170493] (d) Agbasi-Porter C, Ryman-Rasmussen J, Franzen S, Feldheim D. Bioconjugate Chem. 2006; 17:1178–1183.

(14). Seferos DS, Giljohann DA, Hill HD, Prigodich AE, Mirkin CA. J. Am. Chem. Soc. 2007; 129:15477–15479. [PubMed: 18034495]

(15). Tyagi S, Kramer FR. Nat. Biotechnol. 1996; 14:303–308. [PubMed: 9630890]

(16). Zangmeister RA, Tarlov MJ. Anal. Chem. 2004; 76:3655–3659. [PubMed: 15228337]

(17). Hurst SJ, Lytton-Jean AKR, Mirkin CA. Anal. Chem. 2006; 78:8313–8318. [PubMed: 17165821]

(18). Seferos DS, Giljohann DA, Rosi NL, Mirkin CA. ChemBioChem. 2007; 8:1230–1232. [PubMed: 17562553]

(19) (a). Turberfield AJ, Mitchell JC, Yurke B, Mills AP, Blakey MI, Simmel FC. Phys. Rev. Lett. 2003; 90:118102. [PubMed: 12688969] (b) Gidwani V, Riahi R, Zhang DD, Wong PK. Analyst. 2009; 134:1675–1681. [PubMed: 20448937]

(20) (a). Dubertret B, Calame M, Libchaber AJ. Nat. Biotechnol. 2001; 19:365–370. [PubMed: 11283596] (b) Stoermer RL, Keating CD. J. Am. Chem. Soc. 2006; 128:13243–13254. [PubMed: 17017805] (c) You CC, Miranda OR, Gider B, Ghosh PS, Kim IB, Erdogan B, Krovi SA, Bunz UHF, Rotello VM. Nat. Nanotechnol. 2007; 2:318–323. [PubMed: 18654291] (d) Maxwell DJ, Taylor JR, Nie SM. J. Am. Chem. Soc. 2002; 124:9606–9612. [PubMed: 12167056] (e) Dulkeith E, Ringler M, Klar TA, Feldmann J, Javier AM, Parak WJ. Nano Lett. 2005; 5:585–589. [PubMed: 15826091]

(21) (a). Lee OS, Schatz GC. J. Phys. Chem. C. 2009; 113:2316–2321.(b) Lee OS, Schatz GC. J. Phys. Chem. C. 2009; 113:15941–15947.

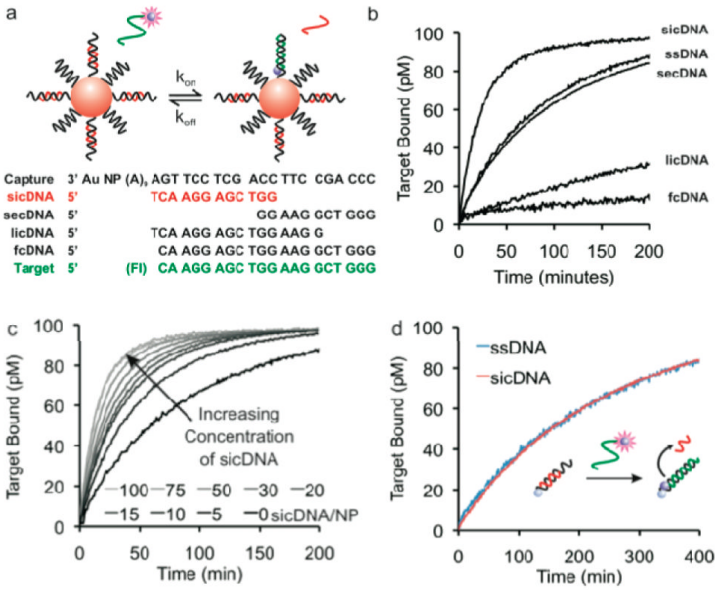

Figure 1.

sicDNA increases the rate of association of DNA–Au NPs to target DNA strands. (a) Scheme depicting the fluorescence-based measurement of a DNA–Au NP binding a target. The corresponding sequences are shown below. (b) Hybridization in the presence of different complements (ssDNA, sicDNA, secDNA, licDNA, and fcDNA). (c) Rate of binding of DNA–Au NPs to targets in the presence of increasing concentrations of sicDNA. (d) Comparison of ssDNA and sicDNA target binding in the absence of the NP. Inset: scheme of the experiment using a molecular quencher. Each plot represents the average of three independent experiments.

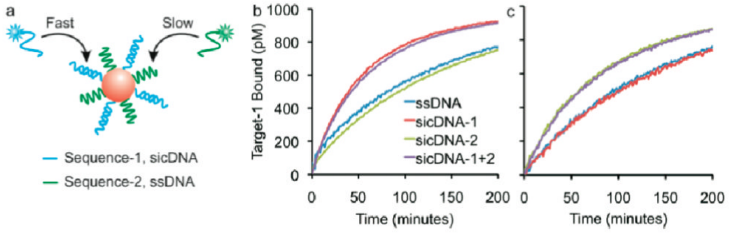

Figure 2.

Effect of sicDNA on the bound strand and adjacent ssDNA sites. (a) Scheme of a nanoparticle containing a mixed monolayer of DNA. The different sequences can be orthogonally addressed by the corresponding sicDNA and target. This experiment was performed in the presence of both target-1 and target-2, which were distinguished by different fluorophore labels. (b) Plot of target-1 binding to DNA–Au NPs in the presence of sicDNA-1 and/or sicDNA-2. (c) Plot of target-2 binding to DNA–Au NPs in the presence of sicDNA-1 or sicDNA-2. Each plot represents the average of three independent experiments.

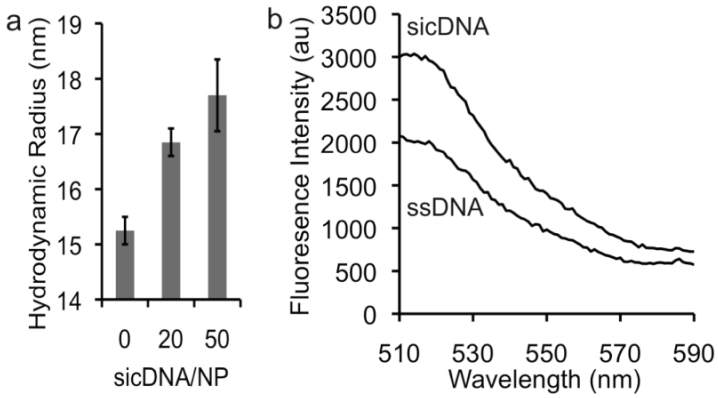

Figure 3.

DNA conformation on the Au NP surface as a function of sicDNA concentration. (a) DLS measurements of the nanoparticle radii at different sicDNA concentrations. (b) Fluorescence spectra from DNA–Au NPs containing a distal fluorophore label. These spectra were taken before and after the addition of sicDNA. Each plot represents the average of three independent experiments. Each error bar represents the standard deviation of the three experiments.

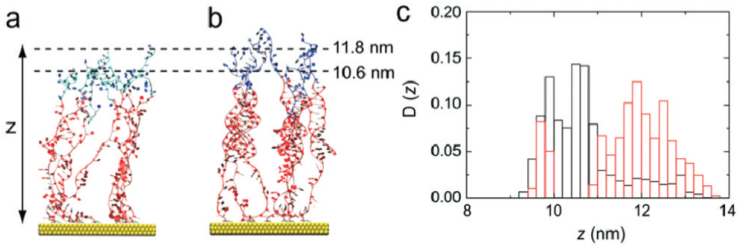

Figure 4.

MD simulation snapshots of ssDNA and sicDNA on flat gold surfaces. Seven strands were modeled on each surface. (a) ssDNA is shown with the final nine residues highlighted in light blue. (b) sicDNA is shown with the final nine residues highlighted in dark blue. (c) Normalized distribution of the distance (*z*) of the last residue of ssDNA (black) and sicDNA (red) from the surface. The average of *z* was 10.6 ± 0.9 nm for ssDNA and 11.8 ± 1.0 nm for sicDNA.

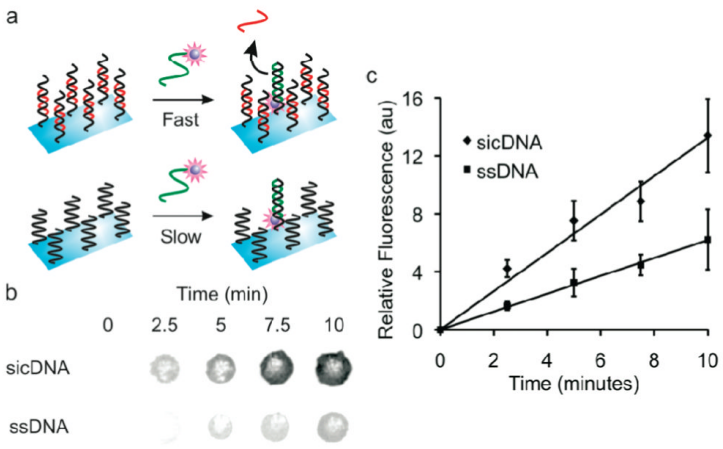

Figure 5.

sicDNA increases the rate of target association on microarrays. (a) Scheme depicting the fluorescence-based detection of target binding to the microarray surface. (b) Fluorescence confocal microscopy images of representative spots after exposure to the labeled target. The reaction was stopped at different time points by washing away unbound target. (c) Quantification of the fluorescence experiments shown in (b). The initial rate of target association was determined by a linear fit of the data. Each error bar represents the standard deviation of four independent experiments.